Cement and Concrete Research 90 (2016) 43–51

Contents lists available at ScienceDirect

Cement and Concrete Research

journal homepage: www.elsevier.com/locate/cemconres

Effect of elevated temperature on alkali-activated geopolymeric binders compared to portland cement-based binders

O.G. Rivera [a], W.R. Long [b], C.A. Weiss Jr. [b], R.D. Moser [b], B.A. Williams [b], K. Torres-Cancel [b], E.R. Gore [b], P.G. Allison [a,*]

[a] Department of Mechanical Engineering, The University of Alabama, Tuscaloosa, AL, United States
[b] US Army Corps of Engineers, Engineer Research and Development Center, Vicksburg, MS, United States

ARTICLE INFO

Article history:
Received 22 September 2015
Received in revised form 9 September 2016
Accepted 12 September 2016
Available online 22 September 2016

Keywords:
Alkali-activated binders
Geopolymers
Elevated temperatures
Mechanical properties
TGA
XRD
CT microtomography

ABSTRACT

This research focused on developing thermally-stable materials based on alkali-activation of slag, fly ash, and metakaolin compared to portland cement mixtures by using a hierarchical approach to material design. At lower length scales, X-ray diffraction (XRD) characterized the mineralogy that coupled to higher length scale experiments using thermogravimetric analysis (TGA) for determining the materials thermal stability. Additionally, high-energy X-ray computed microtomography (μCT) determined the best-performing material formulation that minimized thermal damage when exposed to high temperatures (650 °C). The thermal loading was ramped up to 650 °C from ambient temperature in 60 s and then held for a total of 10 min. The μCT identified that the alkali-activated fly ash mortar had less initial porosity than the ordinary portland cement mixtures, with more than 66% of the pores between 20 and 50 μm in diameter. Consequently, the alkali-activated fly ash mortar was able to dissipate approximately 565 °C in just 50 mm of material, outperforming all the other mixes studied in this paper with μCT confirming minimal damage after the temperature exposure.

1. Introduction

Conventional structural concretes begin losing strength quickly when exposed to temperatures above 300 °C [1]. Typically, a hydrocarbon fire can generate temperatures in excess of 1000 °C with heat fluxes around 150 kW/m^2 within minutes of ignition [2,3]. Additionally, a hydrocarbon jet fuel can have the same temperatures, but the heat flux could be doubled [2,3]. At those temperatures, the compressive strength of portland cement concrete can be reduced by as much as 90% [2]. This loss of strength is commonly attributed to the degradation of the calcium silicate hydrate (C-S-H) as it begins to lose structural water along with dehydration of other hydrates (e.g., calcium hydroxide ($Ca(OH)_2$) and ettringite ($Ca_6Al_2(SO_4)_3(OH)_{12}\cdot 26H_2O$)) and initiation of internal thermal stress gradients. In addition, high-density, high-performance concretes (HPCs) with large amounts of portland cement and low water-to-cementitious materials ratios have issues when exposed to high temperatures. HPCs have a high density with low porosity, and as temperature increases the water vapor is unable to escape, causing pressure to build-up in the pores that results in explosive spalling [4,5]. In cases where HPC is in a confined space, flying debris represents a danger to the personnel responding to fires and sudden failures of supporting structural components create a hazard for the entire structure.

Development of a cementitious material capable of withstanding elevated temperatures due to extreme environments is required for a variety of civilian and military applications. Currently, an environmentally-friendly construction material capable of retaining mechanical performance at elevated temperatures is being developed that also reduces the amount of carbon dioxide emissions into the atmosphere. Instead of using portland cement as the binding component, industrial by-products such as fly ash, slag, and/or metakaolin are being incorporated to create a geopolymeric composite material [6–12]. A review of the geopolymer technology prepared by Duxson et al. [13] concluded that a significant amount of research has been performed, however, considerably more research is required to advance the technology to commercial applications. Geopolymer technology has the capacity for wide-scale applications in the construction industry, as well as in other applications due to similar engineering properties of portland cement and in some cases better thermal properties.

Research by Zhao and Sanjayan [14] has shown that geopolymer concretes consisting of non-hydrated aluminosilicate gel binding phases combined with thermally-stable aggregates have survived exposure to fire testing, while similar portland cement concrete structures have failed. Side-by-side experiments of geopolymer and portland cement concretes designed to have comparable compressive strengths revealed that the geopolymer concrete has a higher fire spalling resistance than the portland cement-based concretes. Zhao and Sanjayan [14] attributed this spalling resistance to a highly porous structure that

* Corresponding author.
E-mail address: pallison@eng.ua.edu (P.G. Allison).

http://dx.doi.org/10.1016/j.cemconres.2016.09.013
0008-8846/

facilitates the release of the internal steam pressure build-up after exposure to the elevated temperatures.

The research by Zhao and Sanjayan built upon the progress made by Duxson et al. [13] and Kong and Sanjayan [15] that showed that alkali-activated aluminosilicate gels present in aluminosilicate-based concretes are inherently different from portland cement-based concrete. The use of these type of binders requires a sodium and/or potassium-based alkali source that reacts with silica- and alumina-rich phases (e.g., clays and glasses), which results in a gel that does not contain the large amounts of chemi- or physi-sorbed water when compared with C-S-H gels produced by portland cement hydration. This open pore structure that distinguishes the aluminosilicate composites reflects the particle sizes of the starting materials [16]. The open pore structure results in a novel inorganic composite material that can withstand temperatures in the range of 600–800 °C with minor loss of strength. Furthermore, Zhao and Sanjayan [14] studied a fly ash based geopolymer and compared the material's response to a portland cement in a simulated gas fire, where the portland cement spalled while the fly ash did not spall.

Some examples of the research on high temperature behavior of metakaolin and fly ash based geopolymers is by Kong et al. [15,17–19], where the Si/Al ratio of the geopolymer was reported as a key parameter influencing the strength reductions after exposing the materials to elevated temperatures. Additionally, Kong reported that elevated temperature curing provided improved compressive strength, while room temperature curing resulted in lower strengths. Kong et al. [17] also reported that the fly ash based geopolymers mixed achieved average ambient compressive strengths of 59.0 MPa, while exposure to an 800 °C elevated temperature increased the strength to 62.8 MPa. This corroborates research done by Pan et al. [20] that showed a fly ash paste exposed to 550 °C had a compressive strength increase of 192% over ambient compressive strengths. Alternatively, Kong et al. [17] also examined metakaolin based geopolymers before and after elevated temperature exposure of 800 °C finding compressive strength decreased from 38.5 to 25.4 MPa.

Cheng and Chiu [21] investigated slag based geopolymers, noticing that strength and fire resistance increased as metakaolin content increased, and reported a 79 MPa compressive strength for the material. Bakharev [22] investigated the thermal stability properties of a fly ash based geopolymer under elevated temperature (800–1200 °C) and found the material to be inappropriate for refractory insulation applications, but added the need for further investigation for fire protection applications.

The thermal deterioration mechanisms reported in these materials are likely due to elevated temperatures above 100 °C leading to the water/moisture in the concrete mixture to vaporize. Once vaporized and unable to escape, leads to cracking and potential catastrophic damage to the infrastructure. To understand this vapor-escaping phenomenon in geopolymer materials, Kong et al. [17] identified that the fly ash based geopolymers have an increased number density of small pores that help the vapor to escape at elevated temperatures. However, metakaolin based geopolymers lack this pore distribution, resulting in damage to the structure [17].

The primary goal of this research was to develop a mixture to withstand elevated temperature exposure and to characterize the damage of these novel aluminosilicate binders using a variety of different analysis techniques. The research presented herein focused on understanding the interaction between gel chemistry and high temperature behavior using thermogravimetric analysis (TGA), X-ray diffraction (XRD), and X-ray computed microtomography (μCT) to identify material composition and infer thermal stability as well as experiments to study the influence of high temperatures on compressive strength and thermal cracking. The goal of this investigation was to identify relevant constituent materials and mixture proportioning considerations to develop castable inorganic composites that are resistant to high temperature exposures.

2. Materials and methods

2.1. Materials

Three alkali-activated mortars fabricated from slag, metakaolin, and fly ash were compared to a portland cement mortar and an ASTM C109 [23] mortar. Slag used in this study met the requirements of ASTM C989 [24], with a specific gravity (SG) of 2.89 coming from the Birmingham slag facility (Birmingham, AL, USA). The fly ash was a low calcium fly ash (Class F), which meets the ASTM C618 Class F [25] and AASHTO M295 Class F [26] requirements. The fly ash had an SG of 2.29 and came from the Bowen power plant (Euharlee, GA, USA). The metakaolin met the requirements of ASTM C618 for a Class N natural pozzolan. The metakaolin is from Advanced Cement Technologies (Blaine, WA, USA) and had an SG of 2.6. The oxide compositions measured using X-ray fluorescence and loss on ignition (LOI) of the above-mentioned materials are given in Table 1.

Alkaline activators used in this investigation consisted of potassium hydroxide and potassium silicate. Potassium hydroxide of ACS reagent grade with purity greater than 85%, was utilized to prepare the activator solutions to a concentration of 14.0 M in deionized water. The solutions cooled for a period of 24 h. following mixing. For the mortar mixtures, a graded silica sand meeting the ASTM C778 [27] requirements was used.

2.2. Sample preparation

Activators were prepared 24 h prior to mixing to allow the activator to reach ambient temperature. The alkali-activated mortars and pastes were prepared adding the liquids to the 11 l tabletop mixer, then the starting material was added slowly (for the mortars, the sand and starting material were dry blended before adding it to the table mixer). Specimens were cast in 76.2 mm × 152.4 mm cylinders for compressive strength testing and 50.8 mm × 101.6 mm cylinders for elevated temperature exposure tests. Samples from all of the mixtures were demolded after 24 h and cured at 23 °C in a moist room except for the fly ash samples, which were sealed in plastic bags and cured in an oven at 40 °C for 72 h. Elevated temperature curing was necessary to harden the fly ash samples. Mixtures were designed for a minimum target compressive strength of 40 MPa at 28 days. The targets for the composition of the activator solution and curing temperatures were determined from previous research [14,18,21,22,28–33]. The two control mixtures were an ASTM C109 [34] mortar with a water to cement ratio of 0.485 and a portland cement mortar (PC/M) with a water to cement ratio of 0.40. The portland cement control mixture was selected, because the cement to sand volume ratio was the same as the other three alkali-activated mortar materials. The alkali-activated mortars were prepared by first adding the liquids then the starting material and the sand. Paste mixtures for TGA and XRD were prepared using the same procedure, but without sand. Thus, there is only one portland cement control paste (PC/P). The alkali-activated slag (S/P), fly ash (FA/

Table 1
Metakaolin, fly ash and slag elemental compositions.

Chemical	Component (wt.%)			
	Metakaolin	Fly ash	Slag	Portland cement type I/II
SiO_2	55.24	53.74	40.92	21.66
TiO_2	1.28	1.40	0.23	0.19
Al_2O_3	39.83	28.26	8.32	2.86
Fe_2O_3	1.83	6.66	0.44	4.47
MgO	0.10	0.91	10.99	2.69
CaO	–	1.38	34.12	63.96
Na_2O	0.04	0.35	0.14	0.09
K_2O	0.26	2.10	0.42	0.24
P_2O_5	0.15	0.26	0.04	0.11
SO_3	–	0.08	2.72	2.74
Loss on ignition	0.32	3.58	0.35	0.81

Table 2
Mixture proportions.

Materials	Mass (%)								
	FA/M	FA/P	M/M	M/P	S/M[a]	S/P	PC/M	C109/M	PC/P
Fine sand	35.92	–	32.26	–	36.78	–	40.04	64.93	–
Fly ash	42.70	66.03	–	–	–	–	–	–	–
Metakaolin	–	–	32.26	47.63	–	–	–	–	–
Slag	–	–	–	–	40.03	61.91	–	–	–
Portland cement	–	–	–	–	–	–	42.83	23.61	71.43
Potassium hydroxide (14 M)	7.82	6.56	6.52	0.96	5.19	7.79	–	–	–
Potassium silicate	11.77	16.45	26.76	39.51	4.79	7.40	–	–	–
Extra water	1.80	10.96	2.21	3.29	12.69	22.67	17.13	11.45	28.57

[a] An inclusion of 0.5% of borax was used to retard the mixture to an acceptable set time.

P) and metakaolin (M/P) pastes where prepared the same way as their similar mortars mixtures. A summary of the mixture proportions used for all materials is provided in Table 2.

2.3. Methods

The following subsections describe the experimental methods used in the research. To more closely simulate concrete, mortar samples were used for compressive strength, elevated temperature, and μCT experiments. However, in order to focus characterization on the paste fraction to determine its thermal stability and phase composition, paste samples that did not contain fine aggregate were used for XRD and TGA measurements.

2.3.1. Compressive strength testing

Compressive strength testing was performed using a servo-hydraulic controlled, 2000kN capacity, Baldwin universal testing machine at a constant load rate of 0.25 MPa/s and was controlled using Instron Partner® software version 8.0a wc. At 7, 14 and 28 days of exposure, 75 mm × 150 mm cylindrical test specimens were tested in triplicates for unconfined compressive strength based on the ASTM C39 [23] standard. Two hours prior to testing, specimen ends were capped in accordance with ASTM C617 [35] using a high-strength sulfur compound.

2.3.2. Elevated temperature exposure

The mortar samples were exposed to a 650 °C flame under a military specified rapid rate boundary condition [36]. The thermal dissipation capacity was measured using a data logger to record the temperature

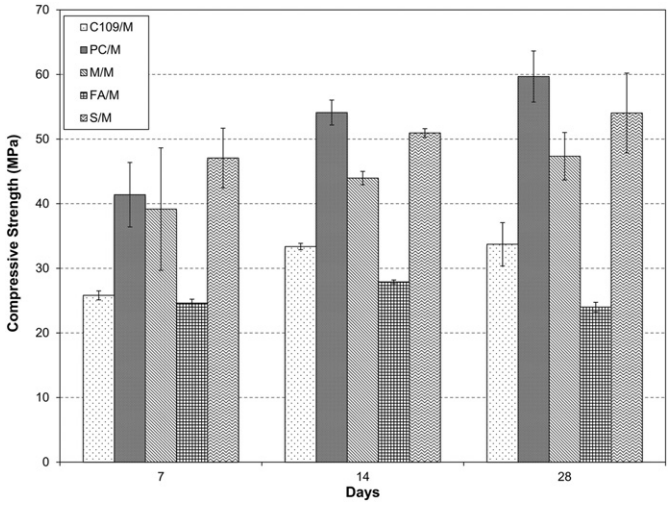

Fig. 2. Comparison of ambient compressive strength results of 7, 14 and 28 days of curing of the different alkali-activated mortars and the control portland cement mortars.

at the 0, 12.5, 50.0, and 82.5 mm vertical locations of the sample when exposed from ambient temperature to 650 °C.

The thermal test fixture was composed of a special Bunsen burner that can achieve temperatures up to 1500 °C while maintaining a steady flame height with minimal temperature fluctuations. The burner used propane gas and contained a vertical stage to control the temperature on the specimen surface. A thermal insulated ceramic board insulated the sides of the sample and prevented the thermocouple wires from becoming damaged by the flame. Temperatures were measured on the surface, and in three vertical locations in the center of the sample as shown in Fig. 1. Samples were tested in triplicates, and heating from ambient to maximum temperature (650 °C) occurred in less than 60 s and it was held for a total of 10 min.

2.3.3. CT microtomography

X-ray μCT data were collected using a Skyscan 1173 High-Energy Micro-CT. The scans were performed using a 130 kV X-ray source operated at 60 μA. A 0.25 mm thick brass filter was inserted to improve resolution and reduce noise. The pixel size selected was 30 μm with an exposure time of 2 s and rotation step size of 0.20°. Reconstructions of the Micro-CT scans were performed using the Skyscan NRecon software in conjunction with the GPUReconServer tool. Smoothing, ring artifact, and beam hardening corrections were made to remove artifacts from

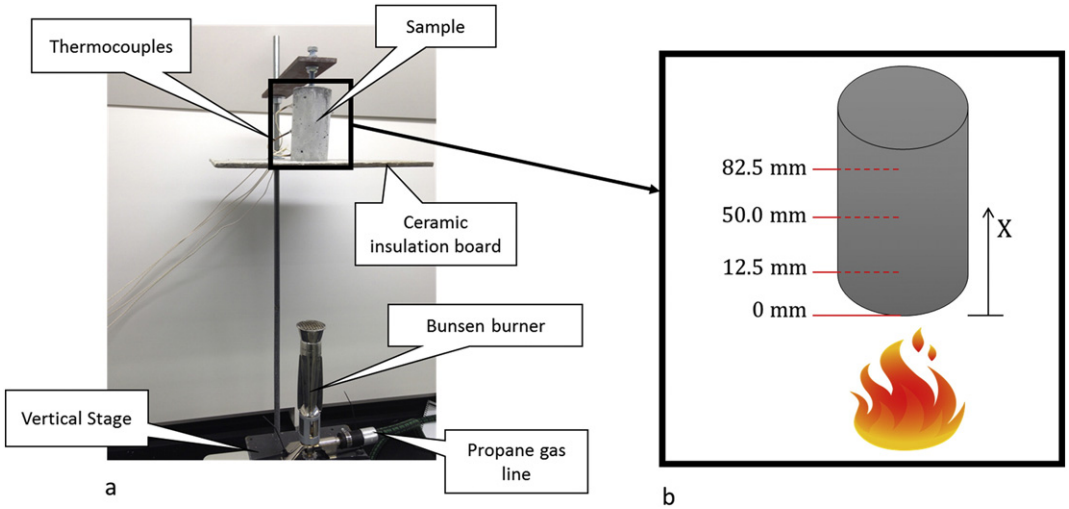

Fig. 1. (a) Schematic of the testing fixture and (b) thermocouple location in the sample (the thermocouples where inserted in the center of the specimen).

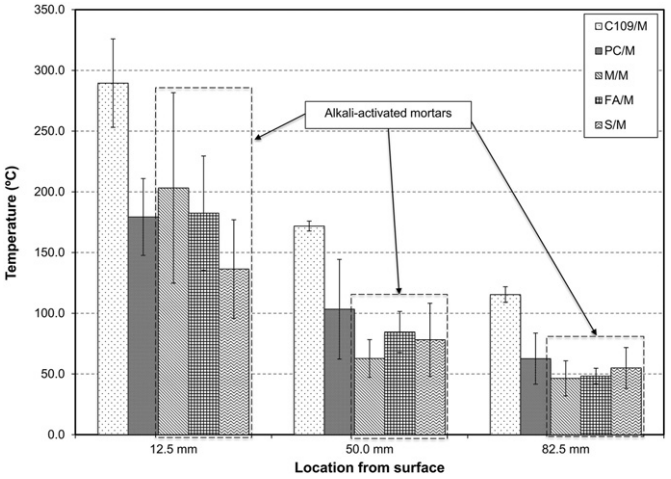

Fig. 3. Comparison of the temperature profiles as a function of spatial location on the sample of the different mixtures.

the reconstructed images. The minimum size detected using the CT microtomography was controlled by the maximum resolution according to the size of specimen scanned, which was 20 μm.

2.3.4. Thermogravimetric analysis (TGA)

TGA was performed using a Netzsch STA 449 *F*1 Jupiter simultaneous thermal analyzer. Approximately 25 mg of ground powder from each sample was immediately inserted in an alumina crucible into the TGA for measurement. Ultra-high purity N_2 was used as the purge gas for all measurements. The temperature was increased from room temperature to 550 °C at a rate of 10 °C/min followed by cooling back to room temperature.

2.3.5. X-ray diffraction (XRD)

In preparation for X-Ray diffraction (XRD) analysis, a portion of material was taken from cores retained from compression stress testing and ground in a Pulverisette (Fritsch Co., Idar-Oberstein, Germany). Each sample was then passed through a 45 μm (No. 325) sieve until at least 90% of the sample passed. Random orientation powder mounts of bulk samples were analyzed using XRD to determine the mineral constituents present in each sample. XRD patterns were gathered from an

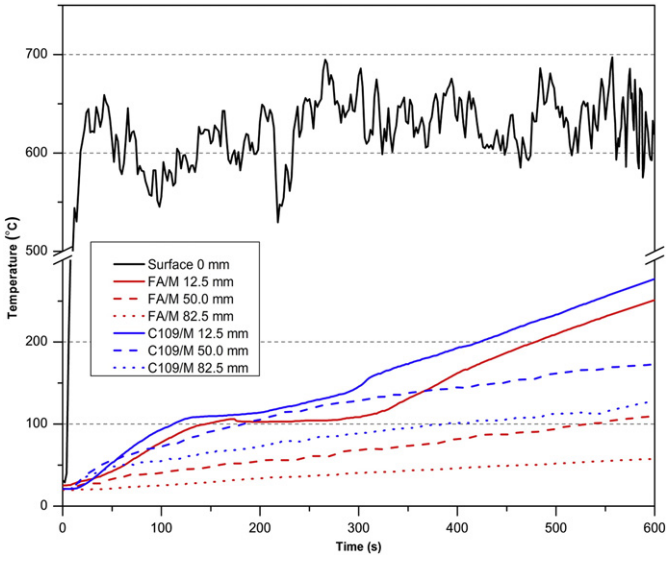

Fig. 4. Temperature profiles as a function of spatial location on the sample, the Surface line (black) illustrates the average temperature profiles of the exposed samples.

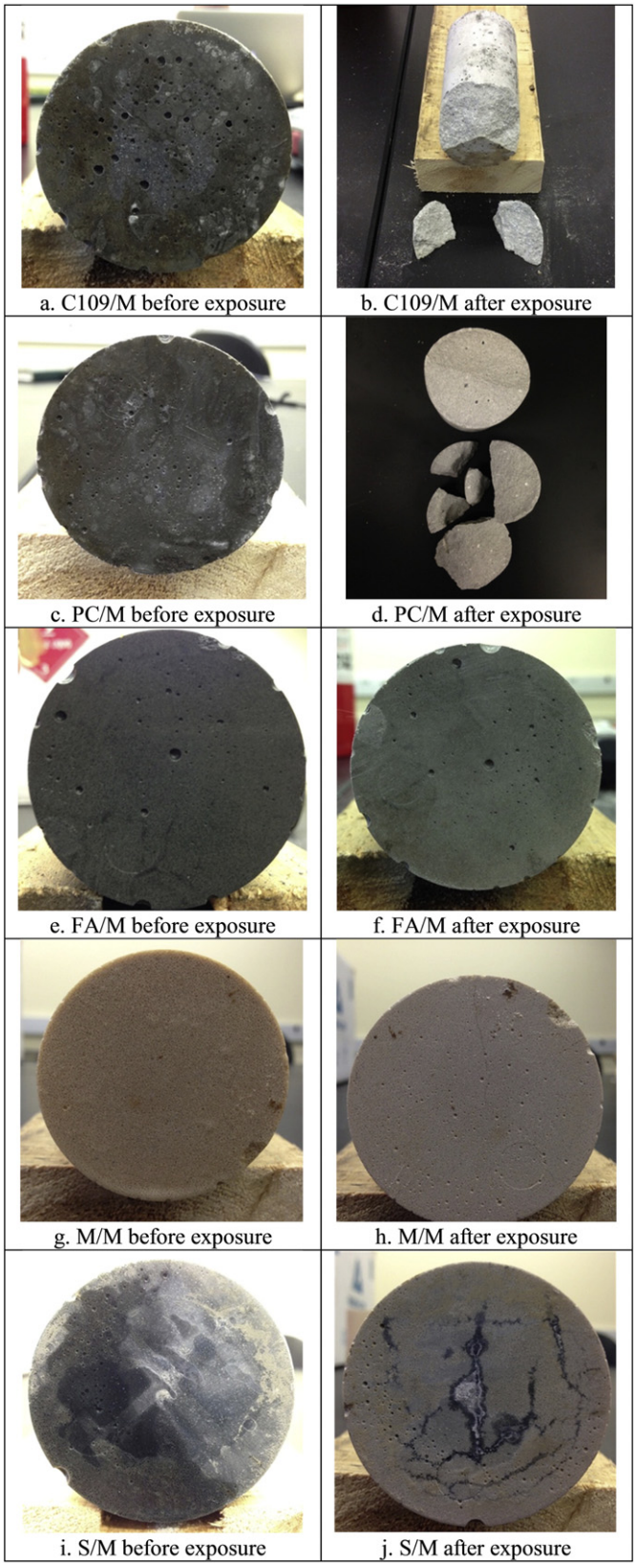

Fig. 5. Before and after thermal exposure with the Bunsen burner of the different mixtures on 50.8 × 101.6 mm cylinders.

X-Pert Pro Multipurpose Powder Diffractometer (Panalytical Inc., Almelo, Netherlands). The run conditions included Co-Kα radiation and scanning (45 kV–40 mA) from 2 to 70°2θ with a step size of approximately

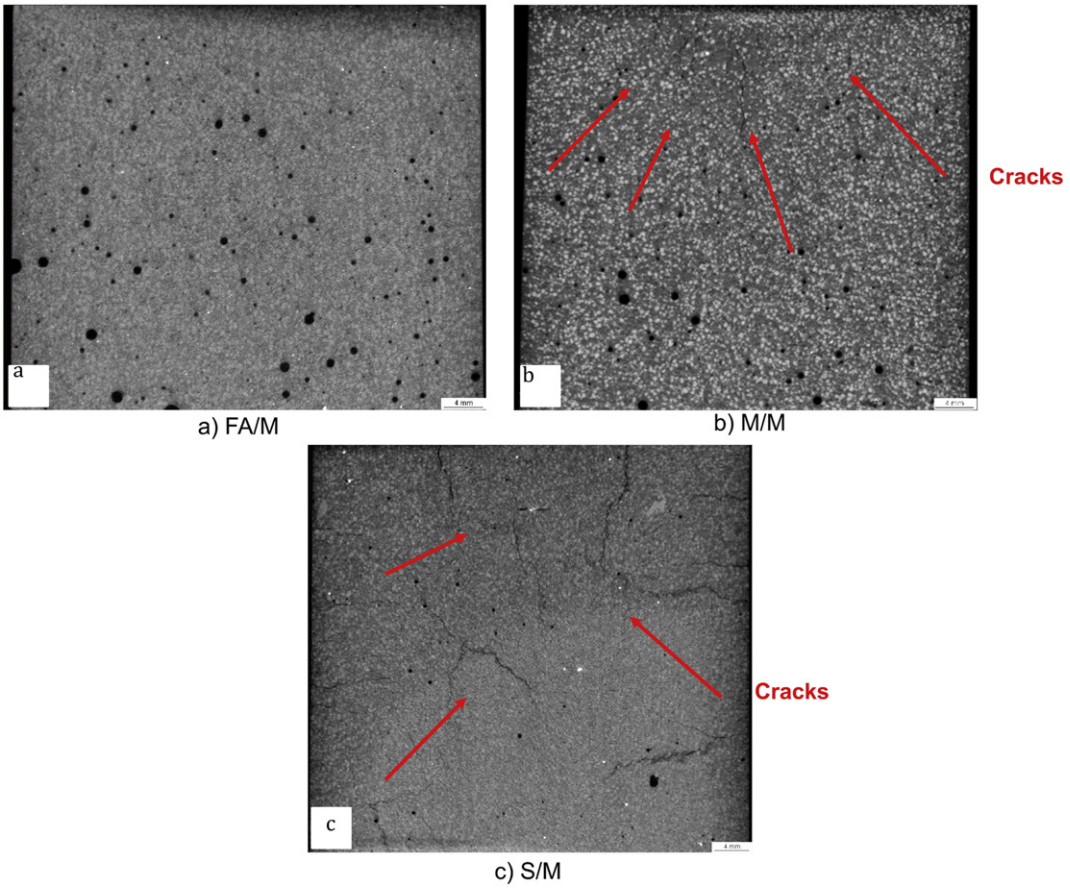

Fig. 6. CT Microtomography of alkali-activated mortars after elevated temperature (650 °C) exposure.

0.002°2θ. Collection of the diffraction patterns was accomplished using the PC-based Windows version of X-Pert Pro Data Collector and analysis of the patterns using the Jade2010 program (Materials Data, Inc.), with patterns from the American Mineralogist Crystal Structure database, International Centre for Diffraction Data, and/or the inorganic crystal structure database.

3. Results and discussion

3.1. Compressive stress testing

All of the compressive strengths increased with age except for the FA/M, as expected for an oven-cured mixture (Fig. 2). Since the FA/M was oven-cured, the compressive strength remained relatively constant exhibiting a similar trend to the data reported by Hardjito [37]. The results in Fig. 2 depict that at 7 days the C109/M and FA/M had comparable values for the lowest ambient compressive strengths, while the S/M had the highest strength. The FA/M sample continued to have the lowest strength out to the 28 days tested at 24 MPa. The PC/M mix ended up with the highest strength after the 28 days of curing followed by the S/M with 60 and 54 MPa, respectively. Both the M/M and the S/M increased with similar increments between 7, 14 and 28 days. After 7 days, only the S/M samples all exhibited strengths greater than 40 MPa. While after 14 days all the PC/M, M/M, and S/M samples had compressive strengths greater than the target of 40 MPa with strength further increasing at 28 days.

Table 3
Air void particle analysis of the alkali-activated mortars before and after exposure compared to portland cement based mortars before exposure.

Sample	Total porosity %		Max (mm)		Average (mm)		Pore count	
	Before	After	Before	After	Before	After	Before	After
FA/M	1.06	1.17	1.05	1.04	0.06	0.06	94,601	101,397
M/M	0.35	0.54	0.99	1.00	0.09	0.05	11,320	62,292
S/M	0.08	0.40	1.17	1.21	0.10	0.04	3039	66,068
C109/M	6.24	N/A	2.18	N/A	0.27	N/A	20,686	N/A
PC/M	1.68	N/A	2.27	N/A	0.22	N/A	7349	N/A

N/A – specimen was not analyzed after exposure since it clear visual damage was observed.

3.2. Elevated temperature exposure results

Similar heat transfer trends were seen in all the mixtures (Fig. 3), showing reductions in the heat transferred through the depth of the cylinder at the three different vertical locations measured. Nonetheless, the heat transferred through the sample was not related to propensity for thermal cracking. All three alkali-activated mortars exhibited lower heat transfer at 82.5 mm of depth compared to the C109/M and PC/M. The M/M presented the lowest heat transferred, followed by the FA/M at the maximum depth. Several mixes exhibited cracking or were damaged during the exposure experiments, including the M/M, identifying them as not suitable for the elevated temperature applications. Fig. 4 illustrates the temperature profiles at the different thermocouple locations; where a direct comparison of the fly ash mixture (best performer) and the ASTM C109 (worst performer) are depicted. The best performance was for the fly ash sample, which showed a temperature decrease from the surface to the middle of the sample of approximately 565 °C. The FA/M behavior can be attributed to its thermally-stable phases and the interconnectivity of internal porosity, which is different than the rest of the mixtures studied and will be discussed in further depth in the following sections.

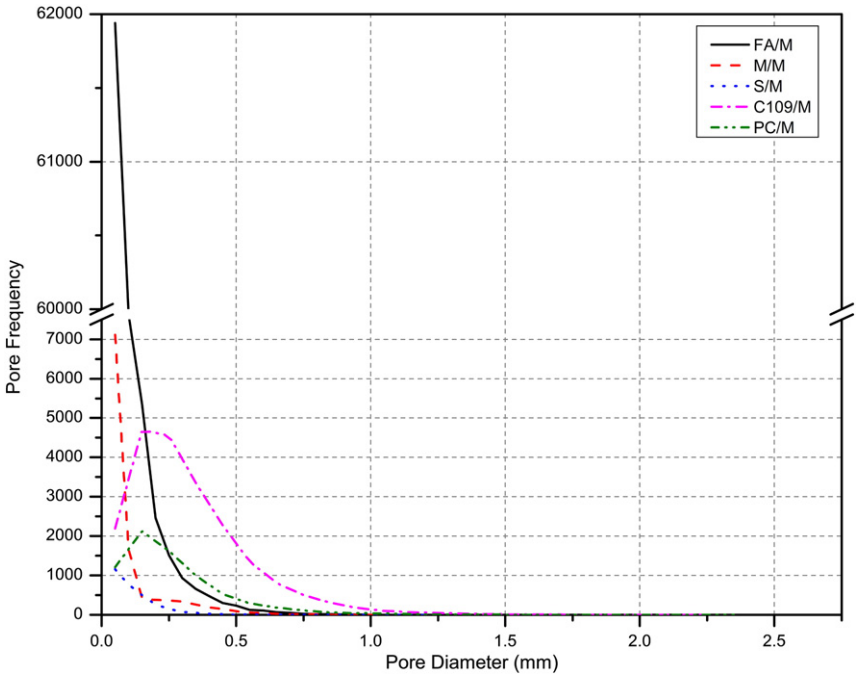

Fig. 7. As-cast comparison of air void distribution for the different mixtures.

3.3. Characterization of damage

Catastrophic damage during the elevated temperature exposure was visible in two samples, C109/M (Fig. 5a and b) and PC/M (Fig. 5c and d). By comparison, the FA/M (Fig. 5e and f) did not show any visible surface cracking or damage. In contrast, the M/M (Fig. 5g and h) and S/M samples (Fig. 5i and j) both exhibited significant cracking and surface scaling.

3.4. CT microtomography results

Scans of only the alkali-activated mixtures (M/M, FA/M and S/M) were performed after the temperature exposure, since the two control portland cement based mortar mixtures experienced significant cracking and spallation. As seen in Fig. 6a, the FA/M did not display any internal damage, whereas the M/M and S/M in Fig. 6b and c, respectively, displayed internal cracking. When comparing the M/M and S/M to each other, the M/M appeared to exhibit improved high temperature resistance based on the size of crack lengths from the exposed surface. As depicted in the M/M in Fig. 6b, the cracks extend 16.4 mm from the exposure surface, whereas in the S/M in Fig. 6c, the cracks extend 31.5 mm.

Air void analysis was used to compare the pre- and post-elevated temperature exposure CT data. The FA/M mortar mixture had the highest volume fraction of porosity, 1.06%, compared to the other alkali-activated binders, followed by the M/M and then the S/M with 0.35 and 0.08%, respectively. The PC/M and C109/M, had higher percent volume of porosity, 1.68 and 6.24% respectively, than the three alkali-activated binders. Further air void distribution analysis (Table 3, Fig. 7) evidenced that even though the PC/M and the C109/M had higher percent porosity, the FA/M had a higher number of voids than any of the other mixtures, and approximately over 66% (Fig. 7 of these voids are between 0.02 and 0.05 mm in diameter. Fig. 8 displays a 3D reconstruction of the air void distribution of the alkali-activated mortar mixtures before and after exposure. These images also depict some of the cracks generated after exposure to elevated temperatures. The FA/M clearly has a different pore structure than the other mixtures analyzed in this study, and this unique internal pore structure, in addition to more closely packed air voids is possibly one reason for a lower heat transfer.

3.5. Thermogravimetric analysis (TGA)

Results of thermogravimetric analyses of the PC/P, FA/P, M/P, and S/P are provided in Fig. 9. Mass loss vs. temperature results varied greatly for the different materials investigated when tested from the starting temperature of 35 °C to a maximum temperature of 550 °C. The S/P exhibited the greatest mass loss of approximately 16%. This mass loss occurred gradually as H_2O in various states of physi- and chemi-sorption in hydrates volatilized. The DTG curve did evidence deviations from the baseline curve that are likely related to loss of water from various hydrated sulfates. The PC/P evidenced anticipated results with rapid mass loss at approximately 100 °C associated with loss of free H_2O and dehydration of ettringite ($Ca_6Al_2(SO_4)_3(OH)_{12}\cdot 26H_2O$), followed by dehydration of $Ca(OH)_2$ at approximately 450 °C occurring in conjunction with loss of H_2O in various states of sorption in C-S-H. The total mass loss of the PC/P was 12%. The M/P exhibited the next to lowest mass loss of approximately 4.5%. A majority of this mass loss was caused by volatilization of free H_2O from 100 to 300 °C and well absorbed water in aluminosilicate gel phases. The lowest mass loss observed was less than 2% in the FA/P. This mass low was an order of magnitude less than that of the PC/P. A majority of the mass loss in the FA/P occurred by loss of free moisture between 100 and 200 °C, followed by little mass loss associated with primary binding phases present in the FA/P. The results of thermal analysis indicated that the high temperature resistance of the FA/P was highest followed by the M/P, PC/P, and S/P in order of mass loss. The improved performance of the FA/P compared with the other materials studied indicates applicability for use as a high-temperature resistant binder in mortar and concrete. In addition, these results corroborate the results of the other aforementioned experimental results from elevated temperature exposure testing and X-ray computed microtomography measurements that also evidenced the FA/P as the best performing binder for high temperature exposures.

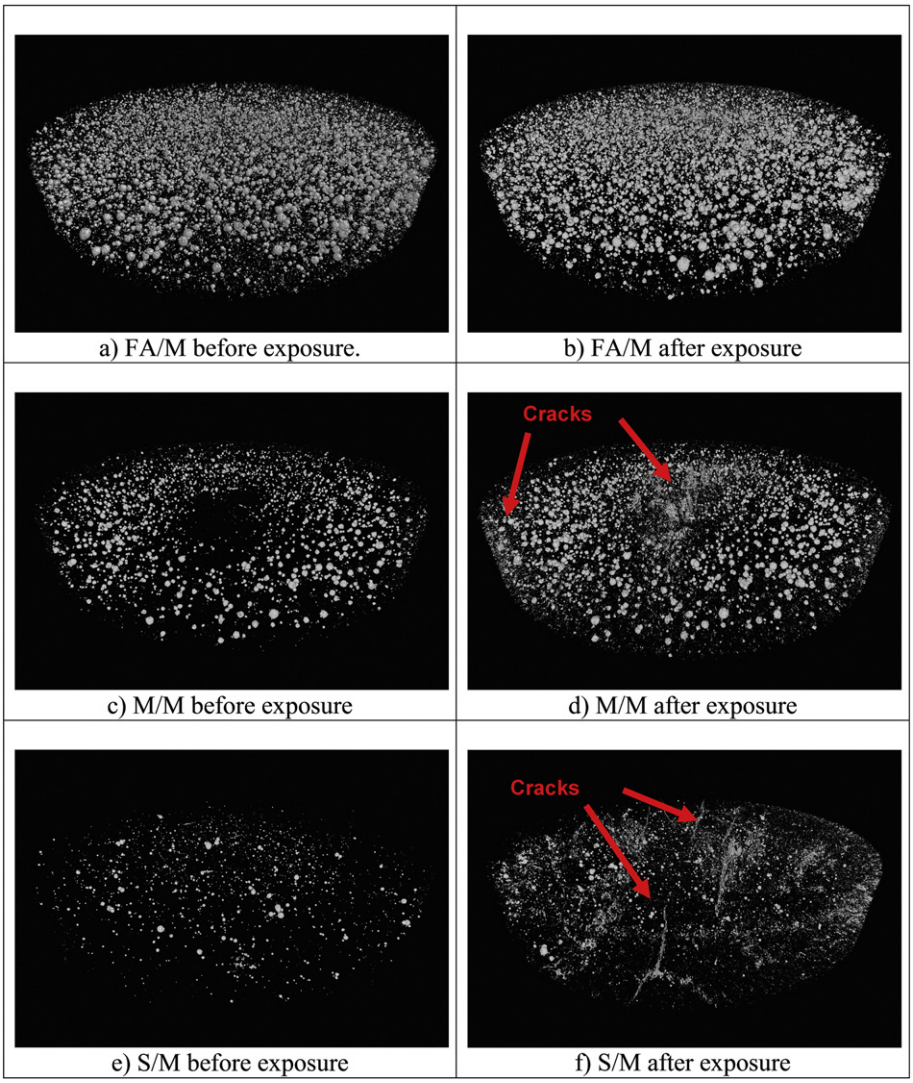

Fig. 8. Generated images showing the air void distribution in a 3d space of the quantified volume (50 × 8 mm) of the three alkali-activated mortars taken using CT microtomography.

3.6. X-ray diffraction (XRD)

Characterization of the phase composition present in PC/P, FA/P, M/P, and S/P paste was accomplished using XRD analysis. The results of XRD analyses for each material investigated are shown as stacked plots (Fig. 10). As expected the phases present in the portland cement paste included ettringite ($Ca_6Al_2(SO_4)_3(OH)_{12}\cdot 26H_2O$), portlandite ($Ca(OH)_2$), various unhydrated cement phases including $Ca_4(Al,Fe)_4O_{10}$ (C_4AF), and Ca_2SiO_4 (C_2S), as well as an amorphous phase attributed to C-S-H. Various hydrates observed are susceptible to high temperature damage by dehydration of hydrated phases as well as potential internal cracking caused by the confined generation of steam at high temperature. The FA/P was composed primarily of an amorphous aluminosilicate gel binder. No phases anticipated to suffer from high temperature damage were observed in the FA/P. The M/P contains amorphous aluminosilicate gel, and remnant phases present in the metakaolin including quartz and anatase. The halloysite and free moisture may cause damage in the M/P when exposed to high temperatures. Finally, the S/P exhibited additional hydrated phases such as hydrocalumite due to the high Ca concentration of the slag and in a way similar to the portland cement-based. The increased abundance of hydrated phases gives rise to reduced high temperature resistance of the S/P. Overall, the results of XRD analyses suggest that the FA/P binder exhibits a phase composition that likely yields the best performance when exposed to high temperatures. The other alkali-activated mixtures and portland cement pastes studied exhibited increased abundance of hydrated phases that likely will reduce high temperature resistance. These hypotheses are supported by the results of other measurements, which have indicated the FA/P as having the least damage following high temperature exposures.

4. Conclusions

This study evaluated the performance of three different alkali-activated mortars and compared them to two different portland cement control mixtures under direct elevated temperature exposure. Findings of this study confirmed that both of the PC/M and the C109/M suffered catastrophic damage under the elevated temperatures, contrary to the alkali-activated mortars (FA/M, M/M and S/M). The FA/M resulted to be the top performer under the specified boundary conditions of 650 °C at a 60 s ramp established for this study. The FA/M did not exhibit any damage after the exposure test. However, both the S/M and M/M out-performed the PC/M and C109/M, even though both S/M and M/M sustained cracks and internal damage. All three alkali-activated mortars demonstrated a greater ability to dissipate heat, but only the FA/M showed up to 565 °C of temperature dissipation in approximately 50 mm of material without thermal cracking.

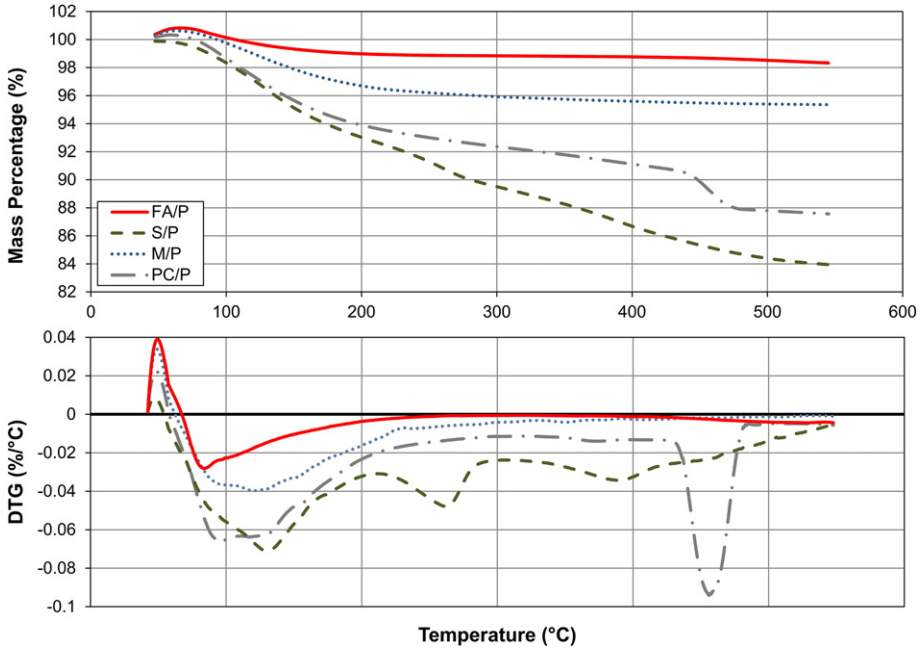

Fig. 9. TG and DTG plot of the different alkali-activated pastes compared to an ordinary portland cement paste.

The pore size and distribution likely contributes to the advantageous performance of the FA/M under elevated temperature environments. A comparison of the thermal data with the CT microtomography pore distribution results for the various mixtures suggests that the pore size, amount and distribution has a sizable effect on the behavior of the FA/M under elevated temperatures. Specifically, the FA/M had a total as-cast air void porosity of 1.1%, exhibiting approximately 66% of the pore diameter ranges between 20 and 50 μm with only a 10% increase in porosity after temperature exposure. While the M/M and S/M samples depicted much lower as-cast porosities, 0.35% and 0.08%, respectively that displayed much larger percent increases in porosity of 54% and 400%, respectively. Additionally, the TGA results identified that the FA/P did not have any phase transformation at the temperatures studied in this paper.

Future research will examine the compressive strengths of the materials before and after exposure to elucidate the influence of the elevated temperature exposure at both quasi-static and high strain rates. Future research will also include nanoindentation before and after temperature exposure to probe the local nanomechanical property changes of the materials.

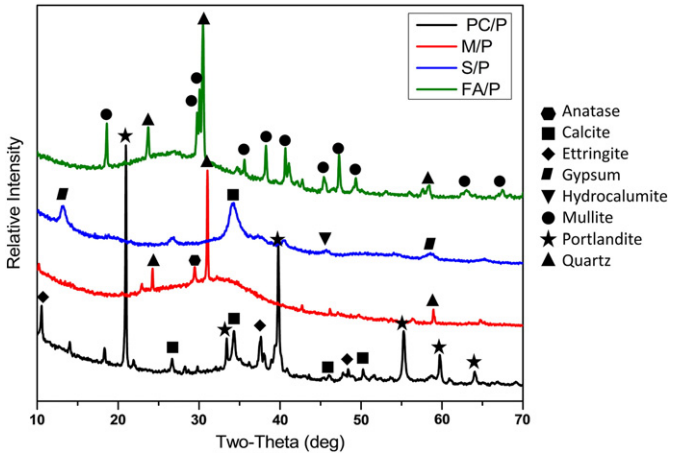

Fig. 10. XRD patterns of the different alkali-activated and the portland cement pastes.

Acknowledgments

Funding for this work was provided by the U.S. Army Engineer Research and Development Center Military Engineering 6.1 Basic Research Program. Permission to publish was granted by Director, Geotechnical and Structures Laboratory, U.S. Army Engineer Research and Development Center.

References

[1] L.T. Phan, N.J. Carino, Fire Performance of High Strength Concrete: Research Needs, NIST, 2000.
[2] European Association for Passive Fire Protection, Hydrocarbon, (1987). http://www.eapfp.com/hydrocarbon.php.
[3] ASTM E1529-14a, Standard Test Methods for Determining Effects of Large Hydrocarbon Pool Fires on Structural Members and Assemblies 1, 2016 1–25, http://dx.doi.org/10.1520/E1529-14A.and.
[4] F.A. Ali, D. O'Connor, A. Abu-Tair, Explosive spalling of high-strength concrete columns in fire, Mag. Concr. Res. 53 (2001) 197–204, http://dx.doi.org/10.1680/macr.2001.53.3.197.
[5] F. Ali, A. Nadjai, D. Talamona, Assessment of the susceptibility of normal and high strength concrete for explosive spalling, J. Appl. Fire Sci. 13 (2005) 79–88.
[6] J. Davidovits, Geopolymer, Chemistry and Applications, 3rd ed Institut Géopolymère, Saint-Quentin, France, 2011.
[7] P.G. Allison, C.A. Weiss, R.D. Moser, A.J. Diaz, O.G. Rivera, S.S. Holton, Nanoindentation and SEM/EDX characterization of the geopolymer-to-steel interfacial transition zone for a reactive porcelain enamel coating, Compos. Part B Eng. 78 (2015) 131–137, http://dx.doi.org/10.1016/j.compositesb.2015.03.011.
[8] R.D. Moser, P.G. Allison, B.A. Williams, C.A. Weiss, A.J. Diaz, E.R. Gore, et al., Improvement in the geopolymer-to-steel bond using a reactive vitreous enamel coating, Constr. Build. Mater. 49 (2013) 62–69, http://dx.doi.org/10.1016/j.conbuildmat.2013.08.001.
[9] A. Fernández-Jiménez, A. Palomo, Composition and Microstructure of Alkali Activated fly ash Binder: Effect of the Activator, 35, 2005 1984–1992, http://dx.doi.org/10.1016/j.cemconres.2005.03.003.
[10] J.M. Miranda, A. Fernández-Jiménez, J.A. González, A. Palomo, Corrosion Resistance in Activated fly ash Mortars, 35, 2005 1210–1217, http://dx.doi.org/10.1016/j.cemconres.2004.07.030.
[11] F. Puertas, T. Amat, A. Fernández-Jiménez, T. Vázquez, Mechanical and Durable Behaviour of Alkaline Cement Mortars Reinforced With Polypropylene Fibres, 33, 2003 2031–2036, http://dx.doi.org/10.1016/S0008-8846(03)00222-9.
[12] F. Puertas, A. Fernández-Jiménez, Mineralogical and Microstructural Characterisation of Alkali-activated fly ash/lag Pastes, 25, 2003 287–292.
[13] P. Duxson, A. Fernández-Jiménez, J.L. Provis, G.C. Lukey, A. Palomo, J.S.J. Deventer, Geopolymer technology: the current state of the art, J. Mater. Sci. 42 (2007) 2917–2933, http://dx.doi.org/10.1007/s10853-006-0637-z.
[14] R. Zhao, J.G. Sanjayan, Geopolymer and Portland cement concretes in simulated fire, Mag. Concr. Res. 63 (2011) 163–173, http://dx.doi.org/10.1680/macr.9.00110.

[15] D.L.Y. Kong, J.G. Sanjayan, Effect of elevated temperatures on geopolymer paste, mortar and concrete, Cem. Concr. Res. 40 (2010) 334–339, http://dx.doi.org/10.1016/j.cemconres.2009.10.017.
[16] A. Hajimohammadi, J.L. Provis, J.S.J. van Deventer, Time-resolved and spatially-resolved infrared spectroscopic observation of seeded nucleation controlling geopolymer gel formation, J. Colloid Interface Sci. 357 (2011) 384–392, http://dx.doi.org/10.1016/j.jcis.2011.02.045.
[17] D.L.Y. Kong, J.G. Sanjayan, K. Sagoe-Crentsil, Comparative performance of geopolymers made with metakaolin and fly ash after exposure to elevated temperatures, Cem. Concr. Res. 37 (2007) 1583–1589, http://dx.doi.org/10.1016/j.cemconres.2007.08.021.
[18] D.L.Y. Kong, J.G. Sanjayan, K. Sagoe-Crentsil, Factors affecting the performance of metakaolin geopolymers exposed to elevated temperatures, J. Mater. Sci. 43 (2007) 824–831, http://dx.doi.org/10.1007/s10853-007-2205-6.
[19] D.L.Y. Kong, J.G. Sanjayan, Damage behavior of geopolymer composites exposed to elevated temperatures, Cem. Concr. Compos. 30 (2008) 986–991, http://dx.doi.org/10.1016/j.cemconcomp.2008.08.001.
[20] Z. Pan, J.G. Sanjayan, F. Collins, Effect of transient creep on compressive strength of geopolymer concrete for elevated temperature exposure, Cem. Concr. Res. 56 (2014) 182–189, http://dx.doi.org/10.1016/j.cemconres.2013.11.014.
[21] T.W. Cheng, J.P. Chiu, Fire-resistant geopolymer produced by granulated blast furnace slag, Miner. Eng. 16 (2003) 205–210, http://dx.doi.org/10.1016/S0892-6875(03)00008-6.
[22] T. Bakharev, Thermal behaviour of geopolymers prepared using class F fly ash and elevated temperature curing, Cem. Concr. Res. 36 (2006) 1134–1147, http://dx.doi.org/10.1016/j.cemconres.2006.03.022.
[23] ASTM C39/C39M-15a, Standard Test Method for Compressive Strength of Cylindrical Concrete Specimens 1, 2016 1–7, http://dx.doi.org/10.1520/C0039.
[24] ASTM C989/C989M-14, Standard Specification for Slag Cement for Use in Concrete and Mortars, West Conshohocken, PA, 2014, http://dx.doi.org/10.1520/C0989_C0989M-14.
[25] ASTM C618-12a, Standard Specification for Coal Fly Ash and Raw or Calcined Natural Pozzolan for Use in Concrete, West Conshohocken, PA, 2012.
[26] AASHTO M 295-11, Standard Specification for Coal Fly Ash and Raw or Calcined Natural Pozzolan for Use in Concrete, 2011.
[27] ASTM C778 - 13, Standard Specification for Standard Sand, West Conshohocken, PA, 2013, http://dx.doi.org/10.1520/C0778.
[28] V.F.F. Barbosa, K.J.D. MacKenzie, Synthesis and thermal behaviour of potassium sialate geopolymers, Mater. Lett. 57 (2003) 1477–1482, http://dx.doi.org/10.1016/S0167-577X(02)01009-1.
[29] V.F.F. Barbosa, K.J.D. MacKenzie, Thermal behaviour of inorganic geopolymers and composites derived from sodium polysialate, Mater. Res. Bull. 38 (2003) 319–331, http://dx.doi.org/10.1016/S0025-5408(02)01022-X.
[30] W.D.a. Rickard, A. van Riessen, Performance of solid and cellular structured fly ash geopolymers exposed to a simulated fire, Cem. Concr. Compos. (2013), http://dx.doi.org/10.1016/j.cemconcomp.2013.09.002.
[31] M.I. Abdul Aleem, P.D. Arumairaj, Optimum mix for the geopolymer concrete, Indian J. Sci. Technol. 5 (2012) 2299–2301.
[32] C. Defazio, M.D. Arafa, P.N. Balaguru, Functional Geopolymer Composites for Structural Ceramic Applications, 2006.
[33] D. Hardjito, M.Z. Tsen, Strength and thermal stability of fly ash-based geopolymer mortar3rd Int. Conf., Curtin University of Technology, Malaysia 2008, pp. 144–150.
[34] ASTM C109/C109M-13, Standard Test Method for Compressive Strength of Hydraulic Cement Mortars (Using 2-in. or [50-mm] Cube Specimens) 1, 2016, http://dx.doi.org/10.1520/C0109.
[35] ASTM C617/C617M-15, Standard Practice for Capping Cylindrical Concrete Specimens 1, 2016 1–6, http://dx.doi.org/10.1520/C0617.
[36] M. Prietto, M. Tsang, S. Hernandez, J. Roepke, D. Piatkowski, E. Lee, et al., The effects of heat damage of aluminum 6061-T6 AM-2 Mats and high power run-up anchor, Eng. Fail. Anal. 18 (2011) 124–137, http://dx.doi.org/10.1016/j.engfailanal.2010.08.014.
[37] D. Hardjito, S.E. Wallah, D.M.J. Sumajouw, B.V. Rangan, On the Development of Fly Ash-Based Geopolymer Concrete, 2005 467–472.